Biophysical Journal Volume 109 November 2015 2148–2158

Article

Interpreting Heterogeneity in Response of Cells Expressing a Fluorescent Hydrogen Peroxide Biosensor

Beijing K. Huang,[1] Sohail Ali,[2] Kassi T. Stein,[2] and Hadley D. Sikes[2,*]
[1]Department of Biological Engineering and [2]Department of Chemical Engineering, Massachusetts Institute of Technology, Cambridge, Massachusetts

ABSTRACT Fluorescent, genetically encoded sensors of hydrogen peroxide have enabled visualization of perturbations to the intracellular level of this signaling molecule with subcellular and temporal resolution. Ratiometric sensors hold the additional promise of meaningful quantification of intracellular hydrogen peroxide levels as a function of time, a longstanding goal in the field of redox signaling. To date, studies that have connected the magnitudes of observed ratios with peroxide concentrations have either examined suspensions of cells or small numbers of adherent cells (~10). In this work, we examined the response of all cells in several microscopic fields of view to an identical perturbation and observed a striking degree of heterogeneity of fluorescence ratios from individual cells. The expression level of the probe and phase within the cell cycle were each examined as potential contributors to the observed heterogeneity. Higher ratiometric responses correlated with greater expression levels of the probe and phase in the cell cycle were also shown to influence the magnitude of response. To aid in the interpretation of experimental observations, we incorporated the reaction of the reduced probe with peroxide and the reactions of the oxidized probe with glutathione and glutaredoxin into a larger kinetic model of peroxide metabolism. The predictions of the kinetic model suggest possible explanations for the experimental observations. This work highlights the importance of a systems-level approach to understanding the output of genetically encoded sensors that function via redox reactions involving thiol and disulfide groups.

INTRODUCTION

Hydrogen peroxide is a signaling molecule important for normal cellular function (1-3) and implicated in pathological conditions such as inflammation and cancer (4-6) as well as neurodegenerative (7) and cardiovascular (8,9) disorders. It acts as a signaling molecule by oxidizing particular cysteine residues of particular proteins (10), and discovering the identities of these proteins is an intense focus of research (11,12). Whether hydrogen peroxide is associated with normal function or pathology, is hypothesized to depend on its spatiotemporal concentration within the cell (13). Due to limitations in methods for measuring intracellular peroxide concentrations reliably (14-17), it has been difficult to definitively test this reasonable hypothesis and, more importantly, establish a quantitative understanding of the signaling networks that characterize particular biological processes. For example, without reliable measurement tools, it is not possible to ask how these networks compare quantitatively across cell types within an organism, different malignant tumors, or even cells within the same tumor.

Knowledge of bacterial and yeast proteins that react specifically with hydrogen peroxide exceeds knowledge of the same within mammalian systems (2). In recent years, genetic engineering has been used to produce fusions of fluorescent proteins with bacterial and yeast proteins that react specifically with hydrogen peroxide (18-20). Fusions are constructed such that changes in the spectrum of the fluorescent protein occur when hydrogen peroxide oxidizes a cysteine of the microbial protein, causing it to subsequently form a disulfide bond with a neighboring cysteine (21,22). Two spectral features are affected, with an excitation peak at one wavelength decreasing and an excitation peak at a second wavelength increasing in a dose-dependent manner upon stimulation with hydrogen peroxide. The ability to examine the ratio of two spectral features, in contrast with measuring changes in fluorescence intensity for only one feature, enables measurements unbiased by the amount of sensor within the cell or the number of cells within a sample.

As part of an ongoing effort to connect the magnitudes of fluorescent, ratiometric responses from a sensor with intracellular concentrations of hydrogen peroxide (23), we have noted with interest the cell-to-cell heterogeneity, captured in part by standard deviations of signals measured from several cells, that has been reported when populations of adherent cells expressing genetically encoded peroxide sensors are stimulated with an identical amount of hydrogen peroxide (19,20). In this work, we explore several hypotheses regarding factors that may underlie this heterogeneity. To do so, we examine larger sample sizes than were typical in past work, and we use a systems model of hydrogen

Submitted April 1, 2015, and accepted for publication August 24, 2015.
*Correspondence: sikes@mit.edu
Beijing K. Huang and Sohail Ali contributed equally to this work.
Editor: Daniel Beard.

0006-3495/15/11/2148/11
http://dx.doi.org/10.1016/j.bpj.2015.08.053

peroxide metabolism within HeLa cells to aid in the interpretation of experimental results. Insights from this analysis support future efforts toward a quantitative understanding of redox signaling in physiological and pathological processes.

MATERIALS AND METHODS

Materials

EMEM (Eagle's Minimum Essential Medium) and FBS (fetal bovine serum) were sourced from ATCC (Manassas, VA). Penicillin-streptomycin was from EMD Millipore (Gibbstown, NJ). HyPer (hydrogen peroxide) plasmid (pHyPer-cyto) was from Evrogen (Moscow, Russia). Lipofectamine was from Life Technologies (Carlsbad, CA). PBS (phosphate-buffered saline), thymidine, and G418 were from Sigma-Aldrich (St. Louis, MO). H_2O_2 was from BDH Chemicals (West Chester, PA). HRP (horseradish peroxidase) and ABTS (2,2′-azinobis [3-ethylbenzothiazoline-6-sulfonic acid]-diammonium salt) were from Alfa Aesar (Ward Hill, MA) and Tokyo Chemicals (Tokyo, Japan), respectively. HeLa cells obtained from ATCC were a gift from Dane Wittrup (Massachusetts Institute of Technology, Cambridge, MA).

Cell culture and transfection

HeLa cells were cultured in EMEM supplemented with 10% FBS (both from ATCC) and 1% penicillin-streptomycin. The cell cultures were maintained in a 37°C humidified incubator in the presence of 5% CO_2. The medium was changed every three days and cells were passaged every 5–6 days.

HeLa cells were stably transfected with pHyPer-cyto vector containing the HyPer gene under CMV promoter. Cells were first transiently transfected with Lipofectamine following the supplier's protocol, in EMEM alone. Twenty-four hours after transfection, the medium was changed to EMEM with 10% FBS and 1% penicillin-streptomycin supplemented with 700 μg/mL of Geneticin selection marker (G418). After two weeks, stable clones were selected by picking fluorescent colonies using a model No. IX81 wide-field fluorescence camera (Olympus, Melville, NY). The selected colonies were expanded in medium containing 200 μg/mL G418 in 96-well plates. The best fluorescing colony was kept for subsequent experiments. The stable HyPer-HeLa cell line was cultured in 200 μg/mL G418 to maintain selection pressure and remove nonfluorescing cells.

The passage number of the HyPer-HeLa cell line was between 3 and 7 for all experiments. For bolus addition and imaging experiments, HeLa cells expressing HyPer were plated at a density of 2×10^4 cells per well for ~42 h in a 96-well plate without G418. Before imaging, each well was washed with prewarmed PBS (pH 7.4), 150 μL of 5–50 μM H_2O_2 in PBS was added to the well, and images were acquired after 10 min at room temperature.

Cell cycle synchronization

For G1/early S phase synchronization, HyPer-HeLa cells were grown as described above in the presence of 2 mM thymidine (24). Control cultures were grown similarly in absence of thymidine. For G0 synchronization, cells were plated at a density of 1×10^4 cells per well in EMEM with 10% FBS. After culturing for 24 h, cells were washed with PBS (pH 7.4) and placed in serum-free media for additional 24 h before imaging (25). Control cultures were grown similarly except the replaced media contained 10% FBS. Cell cycle synchronization was verified using a previously reported method (26).

Imaging

HyPer imaging was done using a wide-field fluorescence microscope (IX81; Olympus) and Lumen 2000 lamp (Prior Scientific, Rockland, MA). Images were acquired with a 20× Olympus objective. The 96-well plate was clamped on the stage to obtain same view-field images before and after the incubation with H_2O_2. HyPer fluorescence images were taken using model No.D415/30x (Chroma Technology, Bellows Falls, VT) and model no. FF01-488/6-25 excitation filters (Semrock, Rochester, NY) while emission was collected using a model No. FF02-525/40-25 filter (Semrock). Both images have 1600×1200 pixel density at 16-bit resolution. Exposure time was set at 300 ms with the lamp intensity at 25%. Images were taken using a Retiga 2000R camera (QImaging, Surrey, British Columbia, Canada). The microscope, lamp, and camera settings were kept constant throughout this study.

Image analysis

HyPer images were background-subtracted using the Rolling Ball algorithm (radius = 200 pixels) in the software ImageJ (National Institutes of Health, Bethesda, MD). These images were then used to identify cell regions in CellProfiler software (Broad Institute, Cambridge, MA) based on intensity thresholding. The thresholding algorithm used was the Mixture of Gaussian Adaptive. The regions determined were filtered using a size criterion of 30–125 pixels and eccentricity of 0–0.9. HyPer ratio for a particular region was calculated as the average pixel intensity in HyPer-long channel divided by the average pixel intensity in HyPer-short channel in that region.

Measuring cellular scavenging of H_2O_2 as a function of time using an HRP-ABTS assay

HyPer-HeLa cells, seeded at 1×10^6 cells in 10 cm^2 dishes, were grown as described above in the absence of G418 for 48 h. Cells were washed with PBS (pH 7.4) and placed in contact with 10 mL of 20 μM H_2O_2 in PBS (pH 7.4). Over a period of 10 min, 150 μL samples were withdrawn every 2 min and placed in a 96-well plate. A quantity of 50 μL of 2.5 mM ABTS and 10 μL of 3 mg/mL HRP was added to each well. Absorbance was measured at 405 nm using a model no. M200 plate reader (Tecan, Männedorf, Switzerland).

Mathematical modeling of the kinetics of reactions of HyPer with H_2O_2 and reductants

The basic framework of the model has been previously reported by Adimora et al. (27). It includes a system of 28 species and ordinary differential equations (ODEs) that describe the kinetics of the network of reactions between H_2O_2, antioxidants, and thiols of proteins within Jurkat cells. We modified certain kinetic parameters and initial conditions of the original model to better represent our cells of interest, HeLa cells. We added a set of redox reactions that describes HyPer's reactivity within this network. All parameters that we modified or added are listed in the Tables S1 and S2 in the Supporting Material. The system of equations governing the rates of reaction of HyPer with H_2O_2 and disulfide reductase species that we added to the model is as follows:

$$\frac{\partial \text{HyPer-(SH)}_2}{\partial t} = -k_{ox}[H_2O_2][\text{HyPer-(SH)}_2] + k_{red}[\text{Grx}][\text{HyPer-SS}] + k_{GRssg}[\text{Grx}][\text{HyPer-SSG}], \quad (1)$$

$$\frac{\partial \text{HyPer-(SOH)}}{\partial t} = k_{ox}[H_2O_2][\text{HyPer-(SH)}_2] - k_s[\text{HyPer-SOH}] - k_{ssg}[\text{GSH}][\text{HyPer-SOH}], \quad (2)$$

$$\frac{\partial \text{HyPer-SS}}{\partial t} = k_s[\text{HyPer-SOH}] - k_{\text{red}}[\text{Grx}][\text{HyPer-SS}], \quad (3)$$

$$\frac{\partial \text{HyPer-SSG}}{\partial t} = k_{\text{ssg}}[\text{GSH}][\text{HyPer-SOH}] - k_{\text{GRssg}}[\text{Grx}][\text{HyPer-SSG}], \quad (4)$$

$$\frac{\partial \text{Grx-SS}}{\partial t} = k_{\text{red}}[\text{Grx}][\text{HyPer-SS}] - k_{\text{GSHssg}}[\text{GSH}][\text{Grx}]. \quad (5)$$

Here, k_{on} is the rate constant for the reaction of HyPer with H_2O_2, k_{red} is the rate constant of the reduction of HyPer-SS by Grx (glutaredoxin), k_s is the rate constant of the formation of the disulfide bond resulting in HyPer-SS, k_{ssg} is the rate constant of the reaction of GSH (glutathione) with HyPer-SOH, k_{GRssg} is the rate constant of the reduction of HyPer-SSG by Grx, and k_{GSHssg} is the rate constant of the reduction of Grx-SS by GSH. We modified the ODEs for H_2O_2, GSH, GSSG, Grx, and Grx-SSG using the appropriate mass balances.

RESULTS

Analysis of fluorescence images

As in past studies (18,22), the genetically encoded sensor HyPer was stably expressed in the cytoplasm of HeLa cells and these cells were stimulated with peroxide via extracellular bolus addition. To measure sensor outputs from individual cells, either fluorescence microscopy or flow cytometry could be employed. However, trypsinization of adherent cells such as HeLa is required for analysis using fluorescence spectroscopy or flow cytometry, and these procedures can cause stress and elevation of reactive oxidative species (28), introducing artifacts. Thus, microscopic analysis is the preferred measurement technique because it leaves the samples unperturbed. Most prior studies that included microscopic image analysis of cells expressing peroxide sensors used small sample sizes (~10 cells) (19,20,29-32). To facilitate analysis of larger sample sizes, we automated the image analysis process, using a combination of ImageJ (National Institutes of Health, Bethesda, MD) and CellProfiler software (Broad Institute). Fig. 1 shows the image processing steps that were used to quantify the HyPer signal from the HeLa cells. A set of two images were obtained for each field of view per time point, using excitation filters centered at 488 nm and 415 nm, with emission collected at 525 nm for both measurements (Fig. 1, *A* and *B*). Images were corrected for uneven illumination using the Rolling Ball algorithm in the software ImageJ (U.S. National Institutes of Health) with a radius of 200 pixels (33). Fig. 1, *C* and *D*, demonstrate that the algorithm allows the elimination of background signal in both excitation channels, and that the level of background signal is quite different in the two channels. After background correction, we aligned each set of images of the same field of view and used the software CellProfiler to identify individual cells expressing HyPer. Cells were identified using a combination of object diameter, eccentricity, and Mixture of Gaussian Intensity-thresholding algorithms, and cells in a cluster are distinguished from one another based on the intensity profile around the cell border (34). (Fig. 1 *E*). Once each cell expressing HyPer was identified, fluorescence ratios within each were calculated by dividing the mean intensity of all pixels within the cell in the 488-nm excitation image by the mean of all pixels within the cell in the 415-nm excitation image. This methodology facilitates rapid analysis of 200–300 cells from multiple sets of images.

Heterogeneity in cellular response to H_2O_2

Fig. 2 shows a representative dose-response experiment when cells are stimulated with hydrogen peroxide and imaged after 10 min. Without exogenous addition of peroxide, all of the cells are characterized by similar fluorescence ratios near 0.5. When bolus additions of 5–20 μM H_2O_2 are used to stimulate the cells, increased HyPer ratios are observed, and above 20 μM H_2O_2, the ratios remain at saturated values and do not increase further. The degree of heterogeneity in the sensor's response in a population of cells to an identical stimulus is striking. For example, a bolus addition of 20 μM H_2O_2 leads to observations of the full range of possible ratios from 0.5 to 3 within the population of cells. We found that this heterogeneity is not unique to HeLa cells, as bolus addition of hydrogen peroxide to human embryonic kidney cells expressing HyPer also caused a heterogeneous response where the signal varied significantly from cell to cell (Fig. S1 *A*). We investigated several possible explanations for these drastically different apparent responses.

Dependence of HyPer response on expression level of the probe and cell cycle

Although HyPer's response is assumed to be independent of expression level, this has not been tested. We tested this assumption by examining the same field of view before and after stimulation by H_2O_2. Fig. 3 *A* shows that in the basal state, a representative 300 cells in addition to those shown in Fig. 2 exhibited HyPer ratios near 0.5. Fig. 3 *B* shows that while the ratios in all cells are similar, the expression level of the sensor in all cells is not. Emission intensity upon excitation centered at 415 nm varies up to 20-fold from the highest expressing cell to the lowest, while emission intensity upon excitation centered at 488 nm varies up to 10-fold. As expected, given that the ratios in all cells are nearly identical, high emission from a cell in one channel correlates with high emission from that cell in the other channel. Thus, emission from either channel before simulation can be used as a measure of the expression level of the fluorescent sensor. Fig. 3 *C* plots the HyPer ratio of 300 cells before stimulation with hydrogen peroxide as a function of

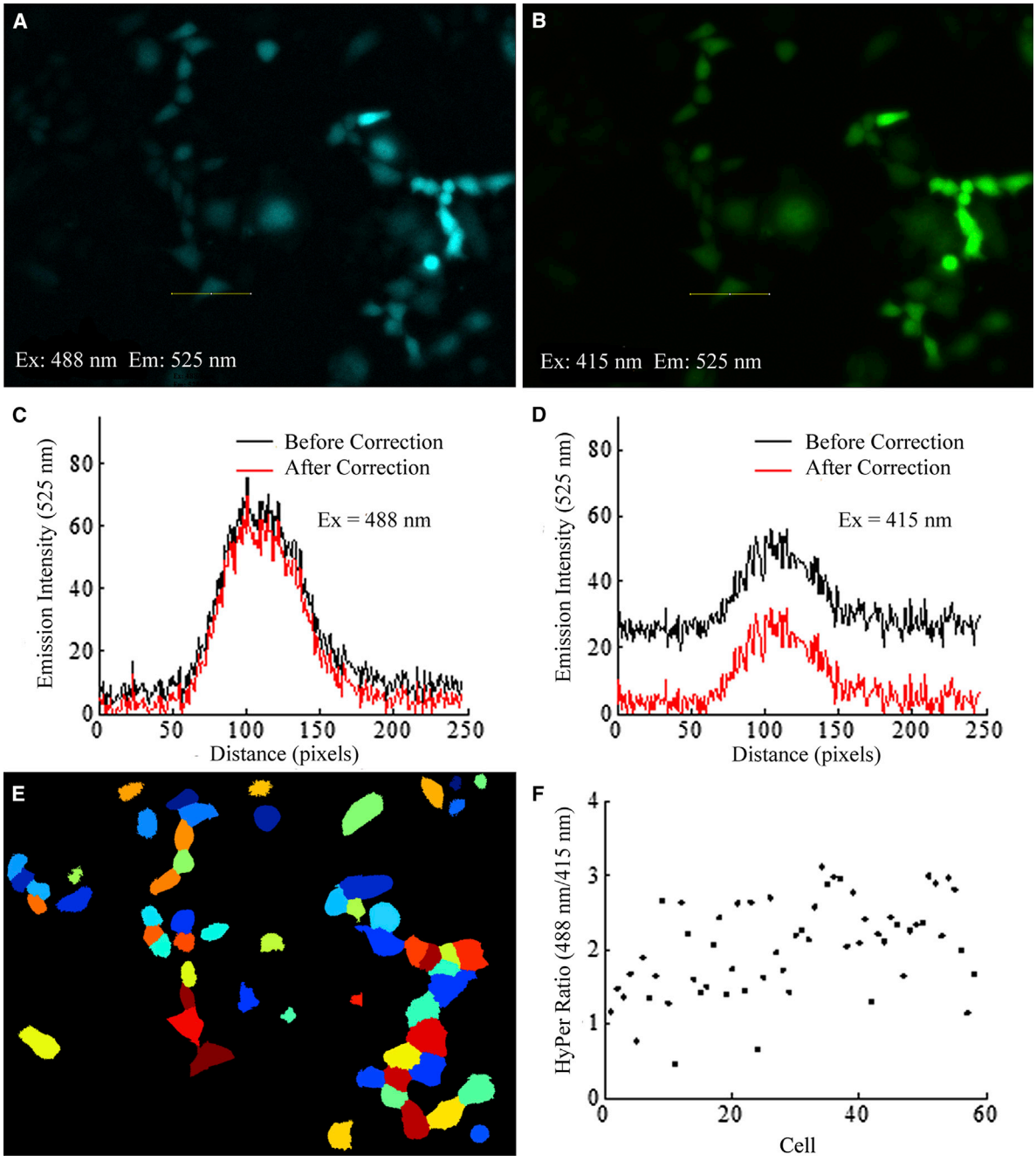

FIGURE 1 Images are processed before calculating the ratiometric HyPer readout. (*A*) Fluorescent image ($\lambda_{ex} = 488$ nm, $\lambda_{em} = 525$ nm) of HeLa cells stably expressing the HyPer sensor protein under control of the CMV promoter. (*B*) Fluorescent image of the same field of view ($\lambda_{ex} = 415$ nm, $\lambda_{em} = 525$ nm). Images shown in (*A*) and (*B*) were taken 10 min after stimulation with 20 μM H_2O_2. (*C* and *D*) Intensity as a function of distance plots for the line shown in (*A*) and (*B*) before and after correction for background signal using the rolling ball algorithm (radius = 200 pixels) in ImageJ. (*E*) Cells expressing HyPer are identified in an automated fashion (CellProfiler) using the background-subtracted image acquired using $\lambda_{ex} = 488$ nm, $\lambda_{em} = 525$ nm. Shading in this image is used to delineate the borders of individual cells. Shading does not indicate the magnitude of fluorescence signals. (*F*) Calculated HyPer ratio for the cells identified in (*E*). The HyPer ratio is defined as the average emission intensity upon excitation with 488 nm light divided by the average emission intensity upon excitation with 415 nm light. Each data point represents the average HyPer ratio within one cell. To see this figure in color, go online.

expression level of the sensor, as indicated by emission upon excitation at 488 nm. Fig. 3 *D* shows the HyPer ratio within these same cells 10 min after stimulation with 20 μM H_2O_2, plotted as a function of emission intensity before stimulation, and it is clear that the magnitude of the observed HyPer response correlates with the expression level of the probe. The leveling off of ratios observed for cells with the highest expression levels of the sensor is due to the fact that the

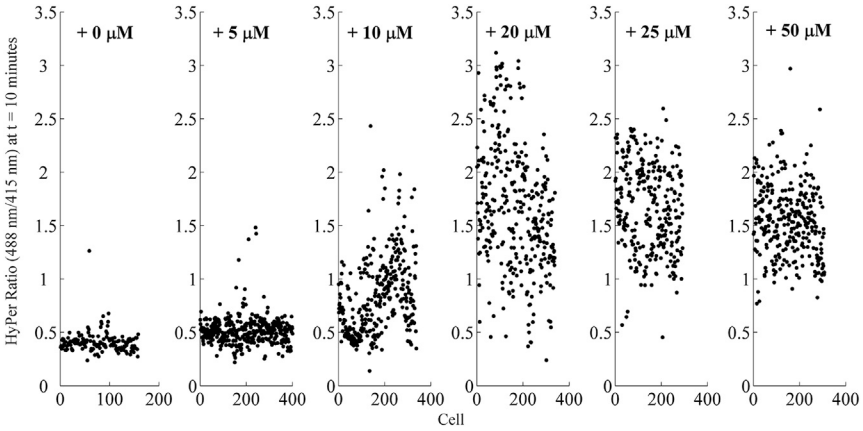

FIGURE 2 The ratiometric response of HyPer to H_2O_2. HyPer-HeLa cells were stimulated with 0–50 μM H_2O_2 and imaged after 10 min. Fluorescence images were obtained using excitation filters centered at 488 and 415 nm. Emission was measured at 525 nm. Each data point represents the HyPer ratio within one cell. Sample sizes are as follows: 0 μM (158 cells), 5 μM (431 cells), 10 μM (337 cells), 20 μM (338 cells), 25 μM (292 cells), and 50 μM (307 cells). Three fields of views were used per condition. Variation in the number of cells for each condition reflects the fact that the number of cells in each field of view varied.

maximum ratio of the HyPer sensor's response has been reached. The Spearman correlation between the emission intensity at time zero and the ratiometric response at 10 min was determined to be 0.70 ($p < 0.05$), signifying that 70% of the variability in the HyPer ratio could be attributed to variation in the expression level of the probe. A similar correlation manifested itself in human embryonic kidney cells expressing the HyPer sensor upon stimulation with an identical bolus addition of hydrogen peroxide (Fig. S1 *B*).

We examined phase within the cell cycle as an additional factor that may contribute to the observed heterogeneity. We synchronized cells in different stages of the cell cycle to determine whether there is a difference in HyPer's response to H_2O_2 as a function of this variable. HeLa cells expressing HyPer were blocked in the G0 phase using serum starvation and in G1/early S phase using 2 mM thymidine (24). The increase in DNA content due to the thymidine arrest was verified by quantifying the DAPI intensity in microscopy images both with and without the blocking agent (26) (Fig. S3). Fig. 4 shows that, upon stimulation with 20 μM of H_2O_2, there was a subtle difference in the distribution of HyPer responses from cells that were blocked in the G0 phase (Fig. 4 *B*) compared to the unsynchronized cell population (Fig. 4 *A*). The difference between HyPer responses of cells that were treated with thymidine and those that were not was more readily apparent. Fig. 4 *D* shows that thymidine-blocked cells exhibited muted responses in comparison to cells that were unsynchronized (Fig. 4 *C*).

These differences are quantitatively elaborated by Fig. 5, a normal probability plot. For cells that were blocked in G1/early S phase using thymidine, the probability of the HyPer ratio within a cell being under 2.5 was 0.99, while for cells that were blocked using serum starvation this probability was 0.9. In contrast, this measure was 0.75–0.8 for unsynchronized cells. In addition, cells that were exposed to media containing thymidine do not have markedly lower expression levels of HyPer as evidenced by the magnitudes of emission intensities before stimulation, so a factor other than expression level of the sensor must be responsible for the observed differences in HyPer responses.

The levels of antioxidant enzymes have been reported to vary with phase within the cell cycle for some cell types

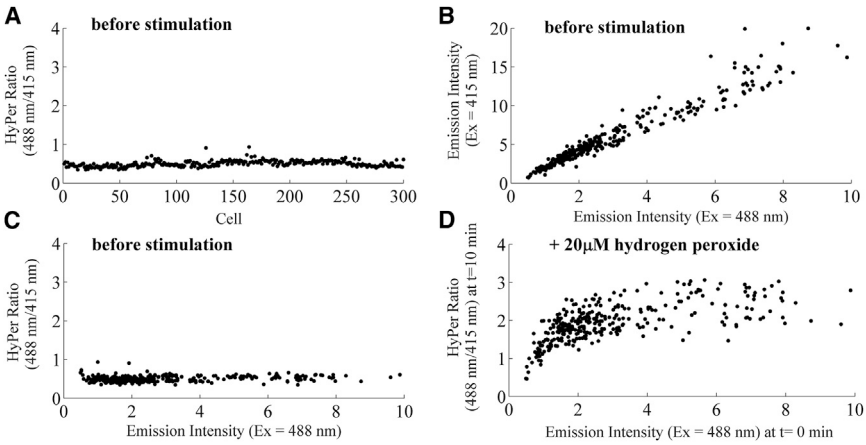

FIGURE 3 HyPer's ratiometric response to H_2O_2 correlates with its expression level. Images of HyPer-HeLa cells were obtained using excitation filters centered at 488 and 415 nm and emission was measured at 525 nm. The same fields of view were imaged before stimulation and 10 min after stimulation with hydrogen peroxide. Each data point represents one cell. (*A*) HyPer ratios within individual cells before stimulation with hydrogen peroxide are relatively uniform. (*B*) Before stimulation, the range of emission intensities within cells indicates expression level of the fluorescent sensor protein, and emission intensity at each of the excitation wavelengths is positively correlated. Emission intensity at either excitation wavelength before stimulation can be used to indicate expression level. (*C*) Before stimulation, the HyPer ratio within each cell does not correlate with the expression level of the sensor. (*D*) Ten minutes after stimulation with 20 μM H_2O_2, the observed HyPer ratio (*y* axis) correlates with the expression level of the sensor within the cell as measured by the emission intensity upon excitation centered at 488 nm before stimulation (*x* axis). All emission intensities were scaled by a factor of 10^4.

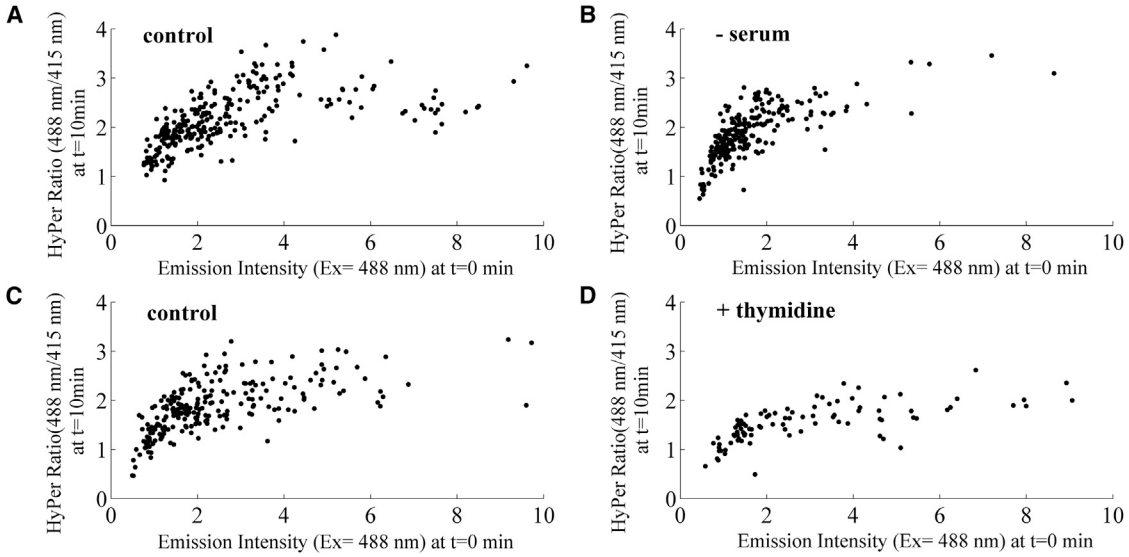

FIGURE 4 Phase within the cell cycle affects HyPer's response. HyPer-HeLa cells were synchronized in G0 phase using serum starvation or in G1/early S phase using 2 mM thymidine. Unsynchronized control cells cultured using complete medium (*A*) and synchronized cells cultured using serum-free medium (*B*) were each identically stimulated with 20 μM H_2O_2 and imaged after 10 min. Similarly, unsynchronized control cells cultured in complete medium without thymidine (*C*) were compared with cells synchronized in G1/early S phase via culture using medium containing 2 mM thymidine (*D*). All emission intensities were scaled by a factor of 10^4.

(35). We reasoned, on the basis of typical expression levels and second-order rate constants for reaction with hydrogen peroxide, that upregulation of these enzymes may reduce the effectiveness of HyPer in the kinetic competition for reaction with hydrogen peroxide, resulting in lower observed HyPer signals. To measure the scavenging capacity of the G1/early S phase cells versus the unsynchronized cells, we compared the rates at which the two cultures removed hydrogen peroxide from the extracellular media. After adding 20 μM H_2O_2 to the cultures, we followed the H_2O_2 concentration remaining in the medium for 10 min. Fitting to a first-order kinetic equation, we compared the decay rates obtained with G1/early S phase synchronized cells with those obtained using unsynchronized cells (Fig. S2). G1/early S phase cells (117 $\pm$ 22 cells per field of view, n = 4 fields) and unsynchronized cells (227 $\pm$ 24 cells per field of view, $n = 6$ fields) each removed H_2O_2 from the media at the same rate, with a decay constant for the entire dish of 0.1 min^{-1}. Because fewer cells in the case of the thymidine-blocked sample contributed to this rate of removal, the data suggest that these cells have a greater capacity for scavenging hydrogen peroxide. One of the ways the decay rate per cell can be increased is if the antioxidant levels inside each cell are upregulated. Therefore, variations in phase within the cell cycle may contribute to heterogeneity in HyPer response, with higher antioxidant levels leading to lower observed ratiometric responses.

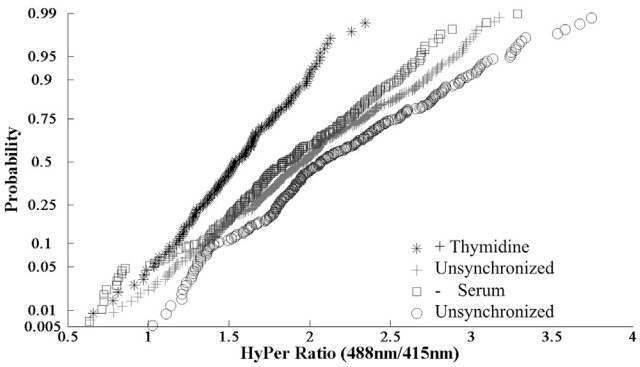

FIGURE 5 A normal probability plot of the data presented in Fig. 4. Phase within the cell cycle has a significant effect on the magnitude of the response of the fluorescent biosensor. All cells were stimulated with 20 μM H_2O_2 and imaged after 10 min. The HyPer ratio is a ratio of emission intensity at 525 nm upon excitation at two different wavelengths, 488 and 415 nm.

Mathematical model of metabolism of hydrogen peroxide by HeLa cells expressing HyPer

To better understand why variations in the expression level of the probe and antioxidant levels within individual cells might cause variation in HyPer's response, we implemented an ODE-based network model simulating the redox reactions of H_2O_2, HyPer, antioxidants, and other proteins within a cell. The network model for H_2O_2 elimination by Jurkat cells reported by Adimora et al. (27) served as a base template, because it included the reactivity of catalase, glutathione peroxidase, peroxiredoxin, and glutaredoxin, the redox reactions of thioredoxin and glutathione, the pseudo-enzymatic oxidative turnover of protein thiols, and the diffusion of H_2O_2 across the plasma membrane. We

adjusted the model for HeLa cells using rate constants and other parameters that we measured in previous work (23). We added reactions of HyPer with H_2O_2, glutathione, and glutaredoxin to the basic framework (Fig. 6 *A*).

The oxidation of HyPer by H_2O_2 occurs at cysteine 199 of the OxyR domain (36). Because of this reaction, HyPer in its reduced state (HyPer-$(SH)_2$) converts to a sulfenic acid form (HyPer-SOH) that can react with cysteine 208 on the same domain to form a disulfide bond (36). This fully oxidized form of HyPer (HyPer-SS) differs significantly in conformation from the reduced form, as evidenced by a change in the excitation spectrum (18). Alternatively, glutathione can react with HyPer-SOH to form a mixed-disulfide form of HyPer (HyPer-SSG) that can be reduced by glutaredoxin (37). For the reduction of the fully oxidized HyPer (HyPer-SS), it has been shown that the disulfide bonds of OxyR are preferentially reduced by the Grx/GSH system (16,38,39). Glutaredoxin can attack the disulfide bond via a dithiol mechanism similar to thioredoxin, resulting in the transfer of the disulfide bond to glutaredoxin and the reduction of HyPer (37,40). The oxidized glutaredoxin (Grx-SS) can then be reduced by GSH (37,40,41). The measured excitation spectrum from a cell expressing HyPer at a particular time point reflects contributions from all of the various oxidation states that are present at that time. Thus, the overall HyPer ratio in a cell is determined by

$$f_{\text{hyper-ss}} \times R_{\text{hyper-ss}} + f_{\text{hyper-ssG}} \times R_{\text{hyper-ssG}} + f_{\text{hyper-(SH)}_2} \times R_{\text{hyper-(SH)}_2} + f_{\text{hyper-SOH}} \times R_{\text{hyper-SOH}},$$

where f is the fraction of the total HyPer that is in a particular oxidation state, and R is the ratio of emission upon excitation at 488 nm to emission upon excitation at 415 nm for that particular state. From the equation, it is evident that changes in the average HyPer ratio are determined by the changes in the fraction of HyPer in each oxidation state. In our model, we simulated the experimental addition of a 20 μM bolus of H_2O_2 outside the cell and followed the kinetics of the HyPer subspecies distributions over time (Fig. 6 *B*), assuming that all of the HyPer are initially in the reduced form (22). Immediately after the addition of H_2O_2, ~80% of the HyPer molecules convert to the HyPer-SSG state while ~20% react to form HyPer-SS. Over a period of 20 min, the fraction of HyPer in these two states decreases as glutaredoxin and glutathione reduces the disulfide bonds and the fraction of HyPer-$(SH)_2$ rises (Fig. 6 *B*). HyPer-SOH represents a negligible fraction of the total HyPer concentration because it is quickly converted to the disulfide or mixed disulfide form. For the purposes of this analysis, we assume that HyPer-$(SH)_2$, HyPer-SOH, and HyPer-SSG have similar excitation spectra because the modifying groups are small and limited to one thiol group, and only HyPer-SS has a significantly different spectrum than that of the reduced form. Thus, changes in the fraction of HyPer in the fully oxidized state are an indirect indication of changes in the overall HyPer ratio.

Typical heterologous expression levels of fluorescent proteins appropriate for detection using fluorescence microscopy result in intracellular, cytosolic concentrations in the range of 0.1–1 μM (42,43). We varied the intracellular concentration of HyPer from 0.1 to 0.5 μM in our model, and plotted the predicted fraction of HyPer-SS as a function of time after the addition of a 20 μM bolus of H_2O_2 (Fig. 7 *A*). We found that increasing the expression level of HyPer increases the fraction of HyPer-SS, and the differences in the fractional value for each expression level becomes

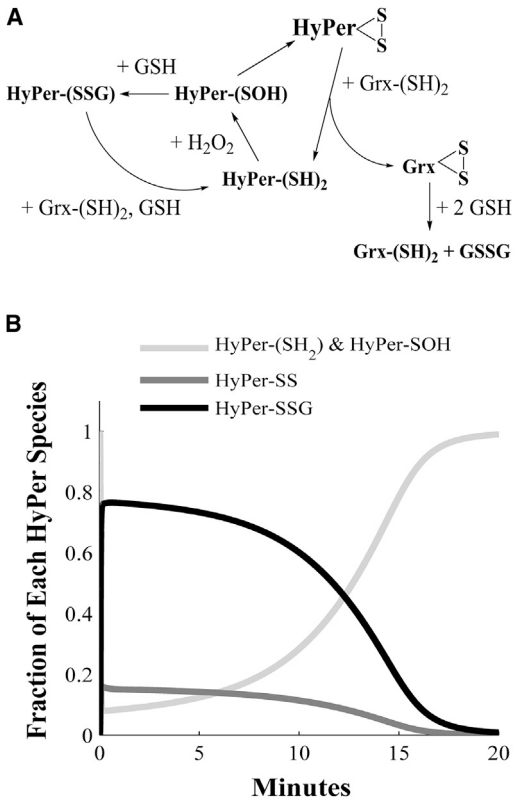

FIGURE 6 Network of HyPer's reactions with H_2O_2 and cellular disulfide reductase species and simulated reaction kinetics. (*A*) Schematic of the HyPer oxidation and reduction through H_2O_2. The reduced form of HyPer (HyPer-$(SH)_2$) is oxidized to the sulfenic form, HyPer-(SOH), through cysteine oxidation at the 199 position. This intermediate species can then form a mix-disulfide bond with GSH to form HyPer-SSG, or it can form a disulfide bond with a nearby cysteine (HyPer-SS), causing a conformational change in HyPer that leads to a different excitation spectrum. Both HyPer-SSG and HyPer-SS are reduced by Grx and GSH back to HyPer-$(SH)_2$. (*B*) Representative figure showing the predicted fraction of each of HyPer's oxidation states over time after stimulation with 20 μM of H_2O_2 bolus. Total HyPer concentration = 0.1 μM. A majority of the HyPer proteins convert to HyPer-SSG almost immediately upon oxidation due to rapid reactions with abundant GSH in the cytoplasm. Slightly <20% convert to the HyPer-SS form. A negligible fraction of the HyPer proteins are in the HyPer-SOH form because it reacts very quickly with a cysteine or a GSH. Over time, the Grx/GSH reduction cycle converts the various oxidized forms of HyPer back to HyPer-$(SH)_2$. We assume that HyPer-SS is the only species that has a different excitation spectrum. Thus changes in the overall HyPer ratio can be represented by fraction of HyPer-SS.

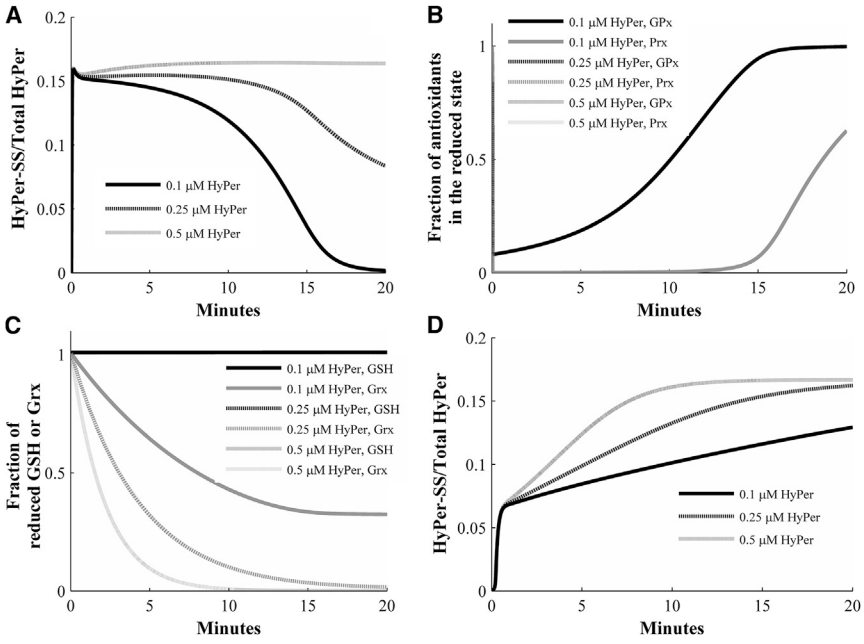

FIGURE 7 Predictions of the impact of variations in HyPer's expression level on the expected oxidation states of HyPer and several antioxidant species as a function of time after stimulation with an extracellular bolus of 20 μM H_2O_2 (*A–C*) or stimulation with continuous, endogenously generated H_2O_2 (*D*). (*A*) Increasing the expression level of HyPer from 0.1 to 0.5 μM changes the fraction of HyPer in the disulfide bond form significantly. (*B*) The effect of increased expression levels of HyPer on the fraction of GPx and Prx in the reduced form over time. Coincident curves show that the expression level of HyPer has no effect on either. (*C*) Effects of an increased expression level of HyPer on the concentrations of GSH and reduced Grx over time. While the GSH concentration did not change, the amount of reduced Grx decreased significantly with higher HyPer expression level. (*D*) The effect of increased expression levels of HyPer on the fraction of HyPer in the disulfide bond for endogenous generation of H_2O_2. Elevating the internal generation of H_2O_2 to 1.1×10^{-5} M/s causes a continuous increase in the fraction of HyPer-SS, and the magnitude of this increase varies with HyPer expression level. Depending on the total HyPer present inside each cell, different HyPer ratios might be measured upon an identical stimulation to all cells.

more significant with time. One hypothesis we investigated is that an increased expression level of HyPer would make it a more effective competitor with the antioxidants inside the cell for H_2O_2. However, when we examined GPx and Prx (peroxiredoxin), two of the dominant H_2O_2 scavengers inside the cell, there is no effect on the magnitude of their interaction with H_2O_2 as measured by the fraction of the GPx and Prx proteins that are in the reduced form in response to the 20 μM bolus (Fig. 7 *B*). Because the expression level of HyPer does not affect the competition at the oxidation step, we examined the effect of HyPer's expression level on the two reduction agents, Grx and GSH. While increasing the concentration of HyPer within the cell does not affect the concentration of GSH in response to the H_2O_2 bolus, it significantly depletes the level of reduced Grx (Fig. 7 *C*). This prediction implies that the reduction of oxidized HyPer is slowed in response to the increased expression of the sensor. Increasing the total expression level of HyPer means proportionally more HyPer molecules can be oxidized; however, the limited amount of reduced glutaredoxin means only a certain number of the disulfide bonds can be reduced at a time, causing an accumulation of HyPer in the oxidized HyPer-SS states, and therefore elevating the overall HyPer ratio. This bottleneck at the reduction step due to Grx causes differences in the fraction of HyPer-SS to become more significant with increased time, because the sensor is more rapidly reduced for lower concentrations of HyPer while at higher concentrations, HyPer remains trapped in the disulfide form.

For the bolus addition of H_2O_2, Fig. 7 *A* suggests that reading the signal at earlier time points may minimize the response differences as a function of HyPer expression levels, before the kinetics of the reduction step play a significant role. However, in many cases of interest, the elevation of H_2O_2 levels is continuous, and following the signal from the sensor over a longer period of time is desirable. In this case, the reduction kinetics become important as shown in Fig. 7 *D*. We simulated the case of internal generation of H_2O_2 and predicted the signal development over a period of 20 min. In this case, the rise in fraction of HyPer-SS is significantly different depending on the expression level of HyPer in the cell.

We further used the model to investigate whether changes in the antioxidant levels of the cell can impact the HyPer ratio, because we found that thymidine-blocked cells had enhanced the H_2O_2 scavenging capacity when we measured the extracellular peroxide removal rate (Fig. S2). Although the experimental measurement revealed an upregulation of a peroxide-eliminating enzyme, it did not specify which one. As an example, we simulated the effect of an increased expression level of one key antioxidant, glutathione peroxidase. The model predicted that the fraction of HyPer-SS decreased as the expression level of GPx increased (Fig. 8). This prediction is consistent with our observation that these synchronized cells exhibited a muted response compared to the unsynchronized cells. The increase in antioxidants decreases the amount of H_2O_2 available to react with HyPer, resulting in a lower overall signal.

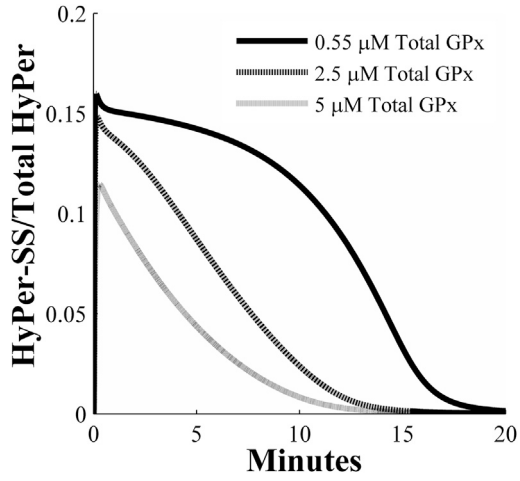

FIGURE 8 The effect of variation in antioxidant expression level on HyPer's oxidation state after stimulation with an extracellular bolus of 20 μM H_2O_2. An increase in GPx concentration in the range of 0.55–5 μM causes a decrease in the fraction of HyPer-SS.

DISCUSSION

The ratiometric property of HyPer and other disulfide redox sensors have long been touted as a way of circumventing problems interpreting data because variations in the expression level of the sensor are not expected to affect the response. However, we found that the expression level of the genetic sensor does affect its ratiometric response to H_2O_2. The higher the expression level of the probe, the higher its percentage residing in the oxidized rather than the reduced form, which results in a higher ratio. Contrary to our initial intuition, the model predicts that an increased expression level of HyPer does not significantly alter its competition with the antioxidant network inside for reaction with H_2O_2, likely because of the slow second-order rate constant of HyPer compared to that of the antioxidants. Instead, our model suggests that there is an imbalance between a rapid oxidation reaction of the sensor by hydrogen peroxide and a slow reduction step once the sensor is oxidized, with the presence of reduced glutaredoxin as the limiting reactant for reduction of oxidized HyPer. This imbalance results in an accumulation of HyPer in an oxidized, disulfide form that increases with the expression level of the probe, while the active depletion of reduced glutaredoxin prevents a proportionate amount of HyPer from being effectively recycled.

Following this logic, the magnitude of the ratiometric signal at the level of the individual cell from other genetic H_2O_2 sensors such as the ro-GFP family may also show a similar dependence on expression level because the disulfide bond of the ro-GFP interacts preferentially with glutaredoxin (16,39). We should note that at the extreme ends of the dose-response curve, this dependence on the expression level is minimized: for bolus H_2O_2 concentrations <1 μM, not enough of the sensor is oxidized to create a kinetic bottleneck during recycling; for bolus H_2O_2 concentrations >20 μM, the residence time of H_2O_2 in the cell is long enough such that much of the sensor is being continually oxidized for a long period of time, and recycling to the reduced state is extremely slow regardless of the sensor expression level. However, these concentrations are outside of the detectable or dynamic range of HyPer. While methods for tracking the amount of reduced Grx in these HyPer-expressing cells are not available as of this writing, antibodies have already been developed against different oxidation states of peroxiredoxin (44,45). We anticipate that in the future, analogous antibodies will be developed for distinguishing between reduced Grx and oxidized Grx, allowing a direct test of the hypothesis that the reduction of oxidized Grx represents a kinetic bottleneck contributing to the correlation of HyPer's ratiometric response with its expression level.

Furthermore, we found that HyPer-expressing cells blocked in the G1/early S phase of the cell cycle respond to H_2O_2 with a muted ratiometric signal in comparison to cells expressing similar levels of HyPer in other phases of the cell cycle. G1/early S phase cells also showed higher H_2O_2 scavenging ability (Fig. S2), implying that they have a higher antioxidant capacity. It is possible that the muted HyPer response to H_2O_2 in G1/early S phase synchronized cells was due to the presence of higher antioxidant levels. We tested this explanation using our model by increasing the concentration of GPx, one of the enzymes that catalyzes the elimination of H_2O_2, and found that an increase in the intracellular concentration of this antioxidant caused a decrease in the fraction of HyPer molecules predicted to be found in the oxidized form (HyPer-SS).

An additional hypothesis for the heterogeneity in HyPer's response from cell to cell is that the basal level of H_2O_2 in HeLa cells varies from cell to cell, perhaps due to phase within the cell cycle, even though differences are undetectable by HyPer. Currently available probes that measure intracellular hydrogen peroxide are recognized as being insensitive to basal levels of H_2O_2 (15). Differences in basal levels may become apparent when H_2O_2 is added to the cells, putting the overall intracellular concentration in the detection range of HyPer. This explanation would suggest that the cell-to-cell variation in H_2O_2 level is on the same order of magnitude as that of the dynamic range of the sensor and a large quantity of valuable information could potentially lie outside of what the probe can measure and detect. Direct measurements of basal H_2O_2 levels will likely become possible in the coming years with the development of improved probes.

Finally, because this study focused on HyPer localized in the cytoplasm, the extent to which the same trend holds for localization of the sensor in other cellular compartments remains to be tested. Certain cellular compartments, such as the endoplasmic reticulum, are highly oxidizing, so the baseline and subsequent dynamic range of the sensor is lessened (22). In addition, fewer measurements are available

regarding the levels of all the species involved in the metabolism of hydrogen peroxide in other compartments, including the level of glutaredoxin. Because the amount of available reduced glutaredoxin may underlie the correlation of the sensor's response with its expression level, we can imagine that a compartment with a higher concentration of glutaredoxin might lead to less cell-to-cell heterogeneity.

CONCLUSIONS

We showed that differences in the expression level of the sensor from cell to cell and phase within the cell cycle can yield very different HyPer ratios in response to the same H_2O_2 stimulus. We explored reasons that may underlie this heterogeneity using a mathematical model and found that a kinetic bottleneck may develop for higher expression levels of the probe due to depletion of the reduced form of glutaredoxin that is responsible for returning the oxidized probe to its reduced form. This heterogeneity suggests that, for questions that are quantitative in nature, caution must be exercised in comparing the responses of small numbers of cells to one another. The automated image processing technique we described allows for unbiased analysis of hundreds of cells from different fields of view, while previous literature that used HyPer for microscopic studies have analyzed typically on the order of 10 cells. We must be careful making inferences based on a few cells, taking into account sensor expression level and cell cycle phase as potential experimental artifacts that can be misinterpreted as indicators of differing magnitudes of change in intracellular peroxide concentration. A quantitative understanding of hydrogen peroxide's role as a cellular signaling molecule will contribute to mechanistic understanding of how networks of reactions control phenotype. To achieve this understanding using genetic sensors, it is important that we measure their outputs with an awareness of the caveats of using these tools to monitor dynamic concentrations of redox-active analytes.

SUPPORTING MATERIAL

Three figures and two tables are available at http://www.biophysj.org/biophysj/supplemental/S0006-3495(15)00994-7.

AUTHOR CONTRIBUTIONS

B.K.H., S.A., K.T.S., and H.D.S. designed the research; B.K.H., S.A., and K.T.S. performed the experiments; B.K.H. contributed analytic tools and performed the kinetic modeling; B.K.H., S.A., and H.D.S. interpreted experimental and theoretical results; and B.K.H., S.A., K.T.S., and H.D.S. wrote the article.

ACKNOWLEDGMENTS

The authors thank Joseph Lim and Troy Langford for critically reading the article.

The authors acknowledge support from a David H. Koch (1962) Fellowship (to S.A. and K.T.S.), a National Science Foundation Graduate Research Fellowship (to B.K.H. and K.T.S.), a Burroughs Wellcome Fund Career Award at the Scientific Interface (to H.D.S.), and the Joseph R. Mares endowed chair in chemical engineering (to H.D.S.).

SUPPORTING CITATIONS

References (46-52) appear in the Supporting Material.

REFERENCES

1. Finkel, T. 2011. Signal transduction by reactive oxygen species. *J. Cell Biol.* 194:7–15.
2. Marinho, H. S., C. Real, …, F. Antunes. 2014. Hydrogen peroxide sensing, signaling and regulation of transcription factors. *Redox Biol.* 2:535–562.
3. Sies, H. 2014. Role of metabolic H_2O_2 generation: redox signaling and oxidative stress. *J. Biol. Chem.* 289:8735–8741.
4. Wiseman, H., and B. Halliwell. 1996. Damage to DNA by reactive oxygen and nitrogen species: role in inflammatory disease and progression to cancer. *Biochem. J.* 313:17–29.
5. Trachootham, D., J. Alexandre, and P. Huang. 2009. Targeting cancer cells by ROS-mediated mechanisms: a radical therapeutic approach? *Nat. Rev. Drug Discov.* 8:579–591.
6. Gorrini, C., I. S. Harris, and T. W. Mak. 2013. Modulation of oxidative stress as an anticancer strategy. *Nat. Rev. Drug Discov.* 12:931–947.
7. Barnham, K. J., C. L. Masters, and A. I. Bush. 2004. Neurodegenerative diseases and oxidative stress. *Nat. Rev. Drug Discov.* 3:205–214.
8. Gao, L., and G. E. Mann. 2009. Vascular NAD(P)H oxidase activation in diabetes: a double-edged sword in redox signalling. *Cardiovasc. Res.* 82:9–20.
9. Al Ghouleh, I., N. K. H. Khoo, …, P. J. Pagano. 2011. Oxidases and peroxidases in cardiovascular and lung disease: new concepts in reactive oxygen species signaling. *Free Radic. Biol. Med.* 51:1271–1288.
10. García-Santamarina, S., S. Boronat, and E. Hidalgo. 2014. Reversible cysteine oxidation in hydrogen peroxide sensing and signal transduction. *Biochemistry.* 53:2560–2580.
11. Sobotta, M. C., W. Liou, …, T. P. Dick. 2015. Peroxiredoxin-2 and STAT3 form a redox relay for H_2O_2 signaling. *Nat. Chem. Biol.* 11:64–70.
12. Rhee, S. G., H. A. Woo, …, S. H. Bae. 2012. Peroxiredoxin functions as a peroxidase and a regulator and sensor of local peroxides. *J. Biol. Chem.* 287:4403–4410.
13. Gough, D. R., and T. G. Cotter. 2011. Hydrogen peroxide: a Jekyll and Hyde signalling molecule. *Cell Death Dis.* 2:e213.
14. Winterbourn, C. C. 2014. The challenges of using fluorescent probes to detect and quantify specific reactive oxygen species in living cells. *Biochim. Biophys. Acta.* 1840:730–738.
15. Ezeriņa, D., B. Morgan, and T. P. Dick. 2014. Imaging dynamic redox processes with genetically encoded probes. *J. Mol. Cell. Cardiol.* 73:43–49.
16. Lukyanov, K. A., and V. V. Belousov. 2014. Genetically encoded fluorescent redox sensors. *Biochim. Biophys. Acta.* 1840:745–756.
17. Rhee, S. G., T. S. Chang, …, D. Kang. 2010. Methods for detection and measurement of hydrogen peroxide inside and outside of cells. *Mol. Cells.* 29:539–549.
18. Belousov, V. V., A. F. Fradkov, …, S. Lukyanov. 2006. Genetically encoded fluorescent indicator for intracellular hydrogen peroxide. *Nat. Methods.* 3:281–286.
19. Gutscher, M., M. C. Sobotta, …, T. P. Dick. 2009. Proximity-based protein thiol oxidation by H_2O_2-scavenging peroxidases. *J. Biol. Chem.* 284:31532–31540.

20. Enyedi, B., M. Zana, …, M. Geiszt. 2013. Spatial and temporal analysis of NADPH oxidase-generated hydrogen peroxide signals by novel fluorescent reporter proteins. *Antioxid. Redox Signal.* 19:523–534.
21. Breckwoldt, M. O., F. M. J. Pfister, …, T. Misgeld. 2014. Multiparametric optical analysis of mitochondrial redox signals during neuronal physiology and pathology in vivo. *Nat. Med.* 20:555–560.
22. Malinouski, M., Y. Zhou, …, V. N. Gladyshev. 2011. Hydrogen peroxide probes directed to different cellular compartments. *PLoS One.* 6:e14564.
23. Huang, B. K., and H. D. Sikes. 2014. Quantifying intracellular hydrogen peroxide perturbations in terms of concentration. *Redox Biol.* 2C:955–962.
24. Bootsma, D., L. Budke, and O. Vos. 1964. Studies on synchronous division of tissue culture cells initiated by excess thymidine. *Exp. Cell Res.* 33:301–309.
25. Lafontaine, J., G. Tchakarska, …, A.-M. Mes-Masson. 2012. Necdin modulates proliferative cell survival of human cells in response to genotoxic stress. *BMC Cancer.* 12:234.
26. Roukos, V., G. Pegoraro, …, T. Misteli. 2015. Cell cycle staging of individual cells by fluorescence microscopy. *Nat. Protoc.* 10:334–348.
27. Adimora, N. J., D. P. Jones, and M. L. Kemp. 2010. A model of redox kinetics implicates the thiol proteome in cellular hydrogen peroxide responses. *Antioxid. Redox Signal.* 13:731–743.
28. Kamarajugadda, S., Q. Cai, …, J. Lu. 2013. Manganese superoxide dismutase promotes anoikis resistance and tumor metastasis. *Cell Death Dis.* 4:e504.
29. Matlashov, M. E., V. V. Belousov, and G. Enikolopov. 2014. How much H_2O_2 is produced by recombinant D-amino acid oxidase in mammalian cells? *Antioxid. Redox Signal.* 20:1039–1044.
30. Miller, E. W., N. Taulet, …, C. J. Chang. 2010. Light-activated regulation of cofilin dynamics using a photocaged hydrogen peroxide generator. *J. Am. Chem. Soc.* 132:17071–17073.
31. Espinosa, A., A. García, …, E. Jaimovich. 2009. NADPH oxidase and hydrogen peroxide mediate insulin-induced calcium increase in skeletal muscle cells. *J. Biol. Chem.* 284:2568–2575.
32. Weyemi, U., O. Lagente-Chevallier, …, C. Dupuy. 2012. ROS-generating NADPH oxidase NOX4 is a critical mediator in oncogenic H-Ras-induced DNA damage and subsequent senescence. *Oncogene.* 31:1117–1129.
33. Hartig, S. M. 2013. Basic image analysis and manipulation in ImageJ. *Curr. Protoc. Mol. Biol.*, Supplement 102:Unit 14.15.1–12.
34. Carpenter, A. E., T. R. Jones, …, D. M. Sabatini. 2006. CellProfiler: image analysis software for identifying and quantifying cell phenotypes. *Genome Biol.* 7:R100.
35. Li, N., and T. D. Oberley. 1998. Modulation of antioxidant enzymes, reactive oxygen species, and glutathione levels in manganese superoxide dismutase-overexpressing NIH/3T3 fibroblasts during the cell cycle. *J. Cell. Physiol.* 177:148–160.
36. Tao, K. 1999. In vivo oxidation-reduction kinetics of OxyR, the transcriptional activator for an oxidative stress-inducible regulon in *Escherichia coli*. *FEBS Lett.* 457:90–92.
37. Berndt, C., C. H. Lillig, and A. Holmgren. 2007. Thiol-based mechanisms of the thioredoxin and glutaredoxin systems: implications for diseases in the cardiovascular system. *Am. J. Physiol. Heart Circ. Physiol.* 292:H1227–H1236.
38. Aslund, F., M. Zheng, …, G. Storz. 1999. Regulation of the OxyR transcription factor by hydrogen peroxide and the cellular thiol-disulfide status. *Proc. Natl. Acad. Sci. USA.* 96:6161–6165.
39. Meyer, A. J., and T. P. Dick. 2010. Fluorescent protein-based redox probes. *Antioxid. Redox Signal.* 13:621–650.
40. Lillig, C. H., and C. Berndt. 2013. Glutaredoxins in thiol/disulfide exchange. *Antioxid. Redox Signal.* 18:1654–1665.
41. Østergaard, H., C. Tachibana, and J. R. Winther. 2004. Monitoring disulfide bond formation in the eukaryotic cytosol. *J. Cell Biol.* 166: 337–345.
42. Tsien, R. Y. 1998. The green fluorescent protein. *Annu. Rev. Biochem.* 67:509–544.
43. Patterson, G. H., S. M. Knobel, …, D. W. Piston. 1997. Use of the green fluorescent protein and its mutants in quantitative fluorescence microscopy. *Biophys. J.* 73:2782–2790.
44. Low, F. M., M. B. Hampton, …, C. C. Winterbourn. 2007. Peroxiredoxin 2 functions as a noncatalytic scavenger of low-level hydrogen peroxide in the erythrocyte. *Blood.* 109:2611–2617.
45. Woo, H. A., S. H. Yim, …, S. G. Rhee. 2010. Inactivation of peroxiredoxin I by phosphorylation allows localized H_2O_2 accumulation for cell signaling. *Cell.* 140:517–528.
46. Peskin, A. V., N. Dickerhof, …, C. C. Winterbourn. 2013. Hyperoxidation of peroxiredoxins 2 and 3: rate constants for the reactions of the sulfenic acid of the peroxidatic cysteine. *J. Biol. Chem.* 288:14170–14177.
47. Kemp, M., Y.-M. Go, and D. P. Jones. 2008. Nonequilibrium thermodynamics of thiol/disulfide redox systems: a perspective on redox systems biology. *Free Radic. Biol. Med.* 44:921–937.
48. Lundberg, M., A. P. Fernandes, …, A. Holmgren. 2004. Cellular and plasma levels of human glutaredoxin 1 and 2 detected by sensitive ELISA systems. *Biochem. Biophys. Res. Commun.* 319:801–809.
49. Kóna, J., and T. Brinck. 2006. A combined molecular dynamics simulation and quantum chemical study on the mechanism for activation of the OxyR transcription factor by hydrogen peroxide. *Org. Biomol. Chem.* 4:3468–3478.
50. Holmgren, A., C. Johansson, …, C. H. Lillig. 2005. Thiol redox control via thioredoxin and glutaredoxin systems. *Biochem. Soc. Trans.* 33:1375–1377.
51. Holmgren, A. 1985. Thioredoxin. *Annu. Rev. Biochem.* 54:237–271.
52. Fernandes, A. P., and A. Holmgren. 2004. Glutaredoxins: glutathione-dependent redox enzymes with functions far beyond a simple thioredoxin backup system. *Antioxid. Redox Signal.* 6:63–74.